Interference-modulated photon statistics in whispering-gallery-mode microresonator optomechanics

Ye Qu,* Jiahua Li,† and Ying Wu‡
School of Physics, Huazhong University of Science and Technology, Wuhan 430074, People's Republic of China

(Received 23 January 2019; published 17 April 2019)

Whispering-gallery-mode (WGM) microresonator optomechanical systems that can attain high quality factors, exhibit small optical mode volume, and can be excited through their evanescent field are versatile platforms for both theoretical and experimental studies in quantum and nonlinear optics. Investigating photon statistical properties in WGM microresonator optomechanical systems is an important avenue to understand their inner interaction mechanism. Here, the interference-modulated photon statistics in a three-mode coupling, i.e., a pair of counterpropagating optical cavity modes and a mechanical mode, in WGM microresonator optomechanical systems is studied. In the case that one optical mode is driven by an external field, strong antibunching photon statistics can be observed in the presence of mode coupling. When the two cavity modes are driven simultaneously, it is found that the photon statistical properties can be well steered by modulating the interference between different transition paths with the help of the amplitudes of the two input fields and their relative phase. Especially, we show in detail that the antibunching photon statistics can be optimized within the weak optomechanical coupling regime by properly adjusting the relative phase. We also find that it is necessary to prepare the mechanical resonator near to the ground state to eliminate the detrimental effect of thermal phonon number on the photon statistical properties. This investigation can deepen our understanding of the interaction between clockwise or counterclockwise light and mechanical motion as well as be useful for the construction of integrated on-chip single-photon sources.

DOI: 10.1103/PhysRevA.99.043823

I. INTRODUCTION

With the rapid development of quantum information science, the study of photon statistics has become a conspicuous focus in quantum physics. One of the benchmarks used to distinguish the properties of photon statistics is the measurement of the second-order correlation function, $g^{(2)}(0)$, at zero-time delay [1,2]. Photons with values of $1 < g^{(2)}(0)$ correspond to super-Poissonian statistics, which is referred to as photon bunching and which is a classical effect, while photons with values of $g^{(2)}(0) < 1$ correspond to sub-Poissonian statistics, which is often referred to as photon antibunching and which is a nonclassical effect. Photon antibunching is a key point for obtaining single-photon sources, which is significant for the realization of distribution, storage, and processing of quantum information in quantum metrology [3], quantum computing [4,5], quantum simulation [6,7], and quantum key distribution [8,9]. In analogy with Coulomb blockades for electrons [10–12], one can also obtain single-photon sources via the physical mechanics of photon blockades and the observation of strong photon antibunching [13]. Many theoretical extensions of photon blockades and photon antibunching have been put forward successively [14–17]. The photon blockade was first observed in a cavity quantum electrodynamics (QED) system by Birnbaum *et al.* [18] in 2005. Thereafter, more and more theoretical [19–23] and experimental advances [24–28] in terms of photon blockades and photon antibunching have been made in different systems, such as quantum dot coupled cavity QED systems [29–31], qubit-cavity coupled systems [32,33], circuit QED systems [34,35], and so on.

In 2010, a new mechanism for photon antibunching as completely opposed to the conventional blockade mechanism described above was invoked by Liew and Savona in a system consisting of two coupled polaritons [36]. It was shown that strong photon antibunching can be achieved with a nonlinearity much smaller than the mode broadening [37–41]. This mechanism is referred to as an unconventional photon blockade because it is based on quantum interference between different excitation pathways from the ground state to the two-photon states [37]. Since 2010, researchers have been committed to the study of unconventional photon blockades in various systems, including, for example, coupled microcavities with second- or third-order nonlinearities [39,42–44], coupled nonlinear photonic molecules [37], Gaussian squeezed states [45], weakly nonlinear photonic molecules [46], coupled quantum dot cavity systems [47], and cavity optomechanical systems [48,49]. More recently, the characteristics of photon antibunching, which is based on quantum interference, have been discussed in detail in bimodal QED by taking into account two different cavity-waveguide arrangements, namely, an inline geometry and a side-coupled geometry [50]. Meanwhile, the unconventional photon blockade has already been realized experimentally in two coupled superconducting circuit resonators [51] and in a quantum dot embedded in a bimodal micropillar cavity [52].

The field of cavity optomechanics, as one of the new directions for the development of quantum optics, has attracted

*quye_1992@126.com
†Author to whom correspondence should be addressed: huajia_li@163.com
‡yingwu2@126.com

considerable attention in recent years. The optical fields in an optomechanical system are coupled to the mechanical modes via radiation pressure, which can be well utilized to manipulate the motion of mechanical resonators and change the properties of cavity fields [53–57]. Many theoretical studies show that cavity optomechanical systems are versatile platforms for studying the statistical properties of photons [58–63]. For instance, under the condition of strong optomechanical coupling, photon blockade or photon antibunching effects can be observed. Unlike in the cavity-QED systems, however, reaching this strong-coupling regime is a long-sought-after goal in cavity optomechanics and beyond the scope of most experiments in the single-photon regime, for which a strong nonlinearity is not easy to realize.

Stimulated by a recent report where phase-modulated photon antibunching in a two-level system coupled to two cavities is proposed [64], in the present paper we investigate tunable photon statistics in a whispering-gallery-mode (WGM) microresonator optomechanical cavity within the weak optomechanical coupling regime. Our system consists of a WGM microresonator and a tapered fiber waveguide, together with two input driving fields. The WGM microresonator contains a mechanically radial breathing mode and two counterpropagating optical WGMs [one clockwise (CW) mode and one counterclockwise (CCW) mode], which are coupled together. The paper mainly focuses on the influences of the coupling of one CW mode to another, which is an expansion on earlier investigation of optomechanically induced transparency (OMIT) based on the coupling of a single stationary mode in the normal mode basis with a mechanical mode [65]. Thus, the photon statistical properties in such a three-mode-coupling WGM microresonator optomechanical system are considered in a more general case. On the one hand, we address the case that only one optical cavity mode is driven by an external input field. Because of the mode-coupling induced quantum interference, strong antibunching photon statistics can be generated. On the other hand, when the two cavity modes of the WGM microresonator are driven by two separated input fields at the same time, one can modulate the quantum interference with the amplitudes of the two input fields and the relative phase between them. Accordingly, the quality of photon statistics can be greatly improved. In particular, we find that the relative phase between the two input fields plays a crucial role in modifying the photon statistical properties of the system. By adjusting the relative phase between the two input fields properly, the photon statistical properties can be well engineered and a high degree of both photon antibunching and superbunching can be obtained. We also give a brief discussion on the influence of thermal photon number on the photon statistics properties. Our obtained results in this paper can be used for photonic interfaces such as single-photon sources.

The remainder of the paper is organized as follows. In Sec. II, the theoretical model and Hamiltonian are described for the three-mode-coupling WGM microresonator optomechanical system. In Sec. III, the output power spectra of the WGM microresonator optomechanical system are presented. Subsequently, in Sec. IV, the zero-time delay second-order correlation function is numerically and analytically discussed. In particular, we analyze and discuss in depth the photon statistical properties of the WGM microresonator optomechanical system for the cases of one input field and two input fields based on detailed numerical simulation results. Finally, summarized discussions and conclusions are given in Sec. V.

II. MODEL AND HAMILTONIAN

As schematically shown in Fig. 1, the system under investigation consists of a WGM microresonator, which is side coupled to an optical tapered fiber waveguide. The WGM microresonator typically supports a pair of counterpropagating modes, namely, CW and CCW modes, with the same decay rate $\kappa = \kappa_{\rm ex} + \kappa_i$ and degenerate frequency ω_0 for symmetry reasons. $\kappa_{\rm ex}$ is the external decay rate (the outgoing coupling coefficient) from the WGM microresonator into the tapered fiber and κ_i is the intrinsic decay rate. More information on the device and experimental details can be found in Ref. [65]. Compared to a previous study where only one of the CW and CCW modes is considered and driven [65], here both of them are simultaneously introduced and driven by the two input fields $\varepsilon_{\rm in}^L = \varepsilon_L e^{-i\omega_L t}$ and $\varepsilon_{\rm in}^R = \varepsilon_R e^{-i(\omega_R t+\theta)}$, respectively. ε_L (ε_R) and ω_L (ω_R) are the amplitudes and angular frequencies of the two input fields. θ represents the relative phase between the two input fields. This relative phase θ is of interest to us, since it can modify the photon statistics of the system (see discussion below). The mode coupling or the normal-mode splitting between these two counterpropagating modes can be realized in the presence of residual scattering of light at the cavity surface or the taper-WGM microresonator contact area by a scattering object [66,67]. Moreover, the WGM microresonator also supports a phonon mode (denoted by operator b) with a mechanical frequency ω_m and a damping rate γ_m. The cavity modes interact with the phonon mode under radiation pressure and the optomechanical coupling strength between

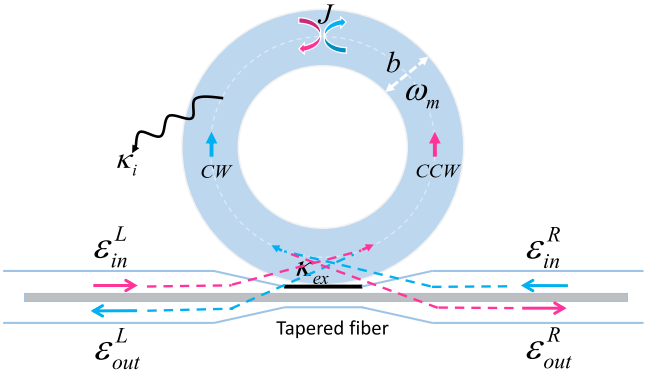

FIG. 1. Schematic diagram of the WGM microresonator optomechanical system which is coherently driven by two input fields through an optical tapered fiber waveguide on both the left- and right-hand ports. The WGM microresonator contains a mechanical radial breathing mode b with a resonance frequency ω_m and two counterpropagating modes (one CW mode $a_{\rm CW}$ and one CCW mode $a_{\rm CCW}$), which are coupled to each other by scattering of light at a rate J because of internal defect centers or surface roughness. The left-hand input field $\varepsilon_{\rm in}^L$ is driven by a coherent light ε_L of frequency ω_L, whereas the right-hand input field $\varepsilon_{\rm in}^R$ is driven by a coherent light ε_R of frequency ω_R with a phase θ with respect to the left-hand input field. The left- and right-hand output fields are described by $\varepsilon_{\rm out}^L$ and $\varepsilon_{\rm out}^R$, respectively. $\kappa_{\rm ex}$ denotes the cavity-waveguide coupling rate and κ_i is the intrinsic cavity decay rate of the two cavity modes.

the cavity modes and the phonon mode at a rate g. In the frame rotating with the left-hand input field frequency ω_L, the Hamiltonian of this three-mode-coupled optomechanical system is described by

$$\begin{aligned}\mathcal{H} &= \hbar\Delta(a_{\rm CCW}^{\dagger}a_{\rm CCW} + a_{\rm CW}^{\dagger}a_{\rm CW}) + \hbar J(a_{\rm CCW}^{\dagger}a_{\rm CW} + a_{\rm CW}^{\dagger}a_{\rm CCW}) \\ &+ \hbar\omega_m b^{\dagger}b + \hbar g(a_{\rm CCW}^{\dagger}a_{\rm CCW} + a_{\rm CW}^{\dagger}a_{\rm CW})(b + b^{\dagger}) \\ &+ \hbar(\varepsilon_L a_{\rm CCW}^{\dagger} + \varepsilon_L^{*}a_{\rm CCW}) \\ &+ \hbar(\varepsilon_R e^{-i\delta t}e^{-i\theta}a_{\rm CW}^{\dagger} + \varepsilon_R^{*}e^{i\delta t}e^{i\theta}a_{\rm CW}), \end{aligned} \tag{1}$$

where $\Delta = \omega_0 - \omega_L$ is the detuning from the frequency ω_L of the left-hand input field to the frequency ω_0 of the two cavity modes. $\delta = \omega_R - \omega_L$ represents the detuning from the left-hand input field frequency ω_L to the frequency ω_R of the right-hand input field. $a_{\rm CCW}$ ($a_{\rm CW}$) and $a_{\rm CCW}^{\dagger}$ ($a_{\rm CW}^{\dagger}$) are the photon annihilation and creation operators of the CCW and CW modes, satisfying the bosonic commutation relations $[a_{\rm CCW}, a_{\rm CCW}^{\dagger}] = 1$ and $[a_{\rm CW}, a_{\rm CW}^{\dagger}] = 1$. Similarly, b and $b^{\dagger}$ are the phonon annihilation and creation operators of the mechanical mode with the bosonic commutation relation $[b, b^{\dagger}] = 1$.

In the above Hamiltonian (1), the first term is the energy of the WGM microresonator in the rotating frame. The second term represents the coherent coupling of the CW mode $a_{\rm CW}$ with the CCW mode $a_{\rm CCW}$, i.e., the so-called mode-coupling term. The third term is the energy of the mechanical oscillator. The fourth term describes the optomechanical coupling due to the radiation pressure with the coupling strength g. The last two terms in Eq. (1) describe the interactions between the cavity field and the two input fields, respectively. One point we want to explain is that we drop the hat of the operator in order to keep the notation as simple as possible. For simplicity and without loss of generality, we assume $\delta = 0$ (i.e., $\omega_R = \omega_L$) for the rest of the paper.

III. OUTPUT POWER SPECTRA OF THE WGM MICRORESONATOR UNDER THE MEAN-FIELD APPROXIMATION

Before discussing the photon statistical properties of the three-mode-coupled WGM optomechanical system, we first consider the system output power spectra. As we know, the structure of the WGM microresonator determines its properties, especially the mode coupling between the two counterpropagating cavity modes. When only one cavity mode is coupled to the waveguide, the other can also be significantly populated due to residual scattering of light at the surface or in the bulk glass [65]. The essence of the phenomenon is the mode coupling between the counterpropagating cavity modes. If the mode coupling satisfies $J \gg \kappa$, the optical resonance splits up and a pair of new eigenmodes which are superpositions of the two counterpropagating cavity modes appears. In this limit, the two cavity modes are well resolved and only one of the new eigenmodes is considered and the other is neglected since it is far-off-resonant and hence not populated [65]. The transmission (P_F) and reflection (P_B) output power spectra can be well used to observe and measure the degree of mode splitting.

According to the Hamiltonian (1) above, the dynamics of the coupled system can be described by the quantum Langevin equations

$$\begin{aligned}\frac{da_{\rm CCW}}{dt} &= -\left(i\Delta + \frac{\kappa}{2}\right)a_{\rm CCW} - iJa_{\rm CW} \\ &- iga_{\rm CCW}(b + b^{\dagger}) - i\varepsilon_L + a_{\rm in}^{\rm CCW}, \end{aligned} \tag{2}$$

$$\begin{aligned}\frac{da_{\rm CW}}{dt} &= -\left(i\Delta + \frac{\kappa}{2}\right)a_{\rm CW} - iJa_{\rm CCW} \\ &- iga_{\rm CW}(b + b^{\dagger}) - i\varepsilon_R e^{-i\theta} + a_{\rm in}^{\rm CW}, \end{aligned} \tag{3}$$

$$\begin{aligned}\frac{db}{dt} &= -\left(i\omega_m + \frac{\gamma_m}{2}\right)b - ig(a_{\rm CCW}^{\dagger}a_{\rm CCW} \\ &+ a_{\rm CW}^{\dagger}a_{\rm CW}) + b_{\rm in}, \end{aligned} \tag{4}$$

where $a_{\rm in}^{\rm CCW}$, $a_{\rm in}^{\rm CW}$, and $b_{\rm in}$ are the input vacuum noises of the cavity modes and phonon mode, respectively. Under the mean-field approximation [68], the quantum fluctuation or thermal noise terms can be dropped, i.e., $\langle a_{\rm in}^{\rm CCW}\rangle = 0$, $\langle a_{\rm in}^{\rm CW}\rangle = 0$, and $\langle b_{\rm in}\rangle = 0$. Here we are interested in the influence of the mode coupling between two cavity modes on the system output power spectra. Thus we assume that there is no coupling between the cavity modes and phonon mode, i.e., $g = 0$. Meanwhile, all of the time derivatives in the quantum Langevin equations are set to be zero. Taking advantage of these operations, it is easy to obtain the analytical steady-state values of the dynamical variables for the two cavity modes as

$$\langle a_{\rm CCW}\rangle = \frac{-i\left(i\Delta + \frac{\kappa}{2}\right)\varepsilon_L - J\varepsilon_R e^{-i\theta}}{\left(i\Delta + \frac{\kappa}{2}\right)^2 + J^2}, \tag{5}$$

$$\langle a_{\rm CW}\rangle = \frac{-i\left(i\Delta + \frac{\kappa}{2}\right)\varepsilon_R e^{-i\theta} - J\varepsilon_L}{\left(i\Delta + \frac{\kappa}{2}\right)^2 + J^2}, \tag{6}$$

although they can be also calculated numerically in the frame of master equations in the Lindblad form [see Eq. (11)].

By using the input-output theory [69,70], the expectation value of the left-hand and right-hand output fields can be obtained as

$$\left\langle \varepsilon_{\rm out}^{R}\right\rangle = \frac{i\varepsilon_L}{\sqrt{\eta_c\kappa}} + \sqrt{\eta_c\kappa}\langle a_{\rm CCW}\rangle, \tag{7}$$

$$\left\langle \varepsilon_{\rm out}^{L}\right\rangle = \frac{i\varepsilon_R e^{-i\theta}}{\sqrt{\eta_c\kappa}} + \sqrt{\eta_c\kappa}\langle a_{\rm CW}\rangle, \tag{8}$$

where $\eta_c = \kappa_{\rm ex}/(\kappa_i + \kappa_{\rm ex})$ is the outgoing coupling parameter, which can be experimentally adjusted by changing the air gap between the WGM microresonator and tapered fiber waveguide. To achieve the best contrast, we choose the critical coupling $\eta_c = 1/2$ as that in Ref. [65]. For the case of $\varepsilon_R = 0$, (i.e., the system is driven only by one input field), the normalized power forward transmission spectra P_F and backward reflection spectra P_B can be expressed as

$$P_F = \frac{\left|\left\langle \varepsilon_{\rm out}^{R}\right\rangle\right|^2}{\left|\frac{\varepsilon_L}{\sqrt{\eta_c\kappa}}\right|^2} = \left|i - \frac{i\eta_c\kappa\left(i\Delta + \frac{\kappa}{2}\right)}{\left(i\Delta + \frac{\kappa}{2}\right)^2 + J^2}\right|^2, \tag{9}$$

$$P_B = \frac{\left|\left\langle \varepsilon_{\rm out}^{L}\right\rangle\right|^2}{\left|\frac{\varepsilon_L}{\sqrt{\eta_c\kappa}}\right|^2} = \left|-\frac{J\eta_c\kappa}{\left(i\Delta + \frac{\kappa}{2}\right)^2 + J^2}\right|^2. \tag{10}$$

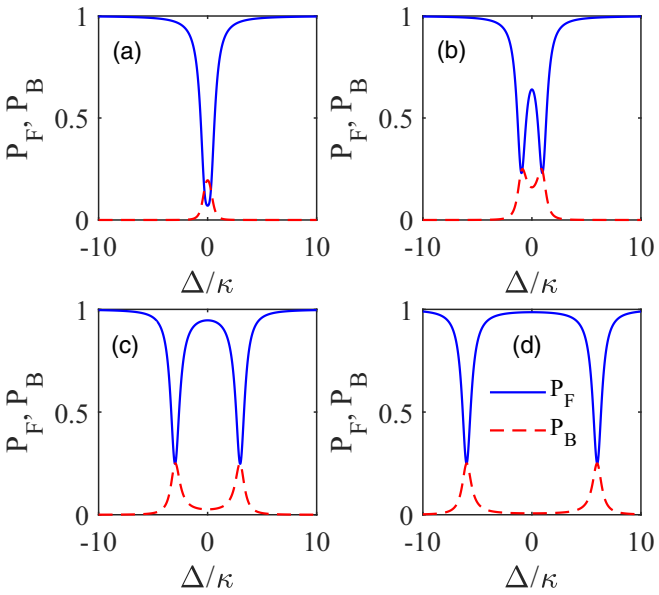

FIG. 2. Calculation results of the normalized power for the forward transmission spectra P_F (blue solid line) and the backward reflection spectra P_B (red dashed line) varying with Δ/κ under the four different values of optical mode-coupling strength J: (a) $J = 0.3\kappa$, (b) $J = \kappa$, (c) $J = 3\kappa$, and (d) $J = 6\kappa$.

Figure 2 displays the normalized power for forward transmission spectra P_F (the blue solid line) and backward reflection spectra P_B (the red dash line) varying with Δ/κ under the four different values of optical mode-coupling strength: (a) $J = 0.3\kappa$, (b) $J = \kappa$, (c) $J = 3\kappa$, and (d) $J = 6\kappa$. From Fig. 2, one can see that the optical resonance splits up and a pair of new eigenmodes appears at $\Delta \pm J$ when $J \geqslant \kappa$. According to the above results, three conclusions can be drawn as follows.

(i) In the weak-coupling regime ($J \leqslant \kappa$), the two cavity modes cannot be resolved.

(ii) In the transition coupling region ($\kappa < J \leqslant 3\kappa$), the two cavity modes can be distinguished but not very well.

(iii) In the ultrastrong-coupling regime ($J \gg \kappa$), a well-resolved mode splitting can be clearly observed in the forward transmission spectra P_F or backward reflection spectra P_B.

That is to say, the two cavity modes can be resolved either in the transition coupling region or in the ultrastrong-coupling regime. For the consideration of making the proposed device suitable for practical operations and applications, we choose $J = 3\kappa$ throughout this paper.

IV. PHOTON STATISTICAL PROPERTIES OF THE WGM MICRORESONATOR OPTOMECHANICAL SYSTEM

A. Second-order correlation function

In order to better study photon statistical properties of the WGM microresonator optomechanical system with the driven-dissipative character, we introduce the quantum master equation for the system density matrix ρ [71]:

$$\frac{d\rho}{dt} = \frac{1}{i\hbar}[\mathcal{H}, \rho] + \kappa\mathcal{L}[a_{\rm CCW}]\rho + \kappa\mathcal{L}[a_{\rm CW}]\rho + \gamma_m(\bar{n}_{\rm th}+1)\mathcal{L}[b]\rho + \gamma_m\bar{n}_{\rm th}\mathcal{L}[b^\dagger]\rho. \quad (11)$$

Here, $\mathcal{L}[O]\rho = \frac{1}{2}(2O\rho O^\dagger - O^\dagger O\rho - \rho O^\dagger O)$ is the Lindblad superoperator term for the collapse operator O acting on the density matrix ρ to account for losses to the environment. $\bar{n}_{\rm th} = [\exp(\hbar\omega_m/k_BT) - 1]^{-1}$ is the mean thermal phonon number of the mechanical bath with the Boltzmann constant k_B and the environment temperature T. In general, the photon statistical properties of the cavity mode $a_{\rm CCW}$ can be distinguished by the measurement of the normalized second-order correlation function

$$g^{(2)}_{a_{\rm CCW}}(0) = \frac{\langle a^\dagger_{\rm CCW}(t)a^\dagger_{\rm CCW}(t)a_{\rm CCW}(t)a_{\rm CCW}(t)\rangle}{\langle a^\dagger_{\rm CCW}(t)a_{\rm CCW}(t)\rangle^2}, \quad (12)$$

at the zero-time delay. This physical quantity emphasizes the joint probability of detecting two photons at the same time. Depending on the value of $g^{(2)}_{a_{\rm CCW}}(0)$, the photon statistical properties of the emitted light field can be distinguished. Values of $g^{(2)}_{a_{\rm CCW}}(0) < 1$ show that the considered cavity field $a_{\rm CCW}$ corresponds to antibunching photon statistics, which is a nonclassical effect. Remarkably, the single-photon regime is usually characterized by $g^{(2)}_{a_{\rm CCW}}(0) < 0.5$. Whereas $g^{(2)}_{a_{\rm CCW}}(0) > 1$ corresponds to the bunching $[2 > g^{(2)}(0) > 1]$ or superbunching $[g^{(2)}(0) > 2]$ photon statistics, which is a classical effect. Once we achieve the density matrix ρ, the mean value of any operator can be computed as $\langle O\rangle = {\rm Tr}(\rho O)$. By solving the master equation in Eq. (11) numerically within a truncated Fock space, the steady-state value of $g^{(2)}_{a_{\rm CCW}}(0)$ thus can be calculated as

$$g^{(2)}_{a_{\rm CCW}}(0) = \frac{{\rm Tr}(\rho_{ss}a^\dagger_{\rm CCW}a^\dagger_{\rm CCW}a_{\rm CCW}a_{\rm CCW})}{[{\rm Tr}(\rho_{ss}a^\dagger_{\rm CCW}a_{\rm CCW})]^2}, \quad (13)$$

where ρ_{ss} is the steady-state solution of the density matrix ρ, which can be obtained by setting $d\rho/dt = 0$ in Eq. (11).

Before the numerical calculations, the approximate analytical solution of the second-order correlation function $g^{(2)}_{a_{\rm CCW}}(0)$ can give a better understanding of the photon statistics from the physical point of view. However, it is very difficult to obtain the analytical expression by directly solving the previous master equation (11). To this end, in the following we utilize the time-dependent Schrödinger equation as an alternative way to provide the analytical description on the properties of the photon statistics. In the weak driving limit, the total excitation number of the considered system is assumed to not exceed 2, as was also done in Refs. [33,37,49]. In this scenario, the truncated state of the system can be approximately expressed as [37]

$$\begin{aligned}|\psi\rangle = {} & C_{0,0,0}|0,0,0\rangle + C_{1,0,0}|1,0,0\rangle + C_{0,1,0}|0,1,0\rangle \\ & + C_{0,0,1}|0,0,1\rangle + C_{1,0,1}|1,0,1\rangle + C_{0,1,1}|0,1,1\rangle \\ & + C_{1,1,0}|1,1,0\rangle + C_{2,0,0}|2,0,0\rangle + C_{0,2,0}|0,2,0\rangle.\end{aligned} \quad (14)$$

Here, $|n_{\rm CCW}, n_{\rm CW}, n_b\rangle$ represents the Fock state with $n_{\rm CCW}$ photons in cavity mode CCW, $n_{\rm CW}$ photons in cavity mode CW, and n_b phonons in mechanical mode b, respectively. $C_{n_{\rm CCW},n_{\rm CW},n_b}$ stands for the probability amplitude and $|C_{n_{\rm CCW},n_{\rm CW},n_b}|^2$ denotes occupying probability in the state $|n_{\rm CCW}, n_{\rm CW}, n_b\rangle$ [33]. Under the weak driving condition, we

have the relations

$$|C_{0,0,0}| \gg |C_{1,0,0}|, |C_{0,1,0}|, |C_{0,0,1}| \gg |C_{2,0,0}|, |C_{0,2,0}|, |C_{1,1,0}|, |C_{1,0,1}|, |C_{0,1,1}|. \tag{15}$$

The values of $C_{n_{\rm CCW},n_{\rm CW},n_b}$ can be solved by substituting Eq. (14) into the Schrödinger equation

$$i\hbar\frac{\partial|\psi\rangle}{\partial t} = \widetilde{\mathcal{H}}|\psi\rangle, \tag{16}$$

where $\widetilde{\mathcal{H}}$ is the effective non-Hermitian Hamiltonian in the zero-temperature approximation [33], given by

$$\widetilde{\mathcal{H}} = \mathcal{H} - i\hbar\frac{\kappa}{2}(a^\dagger_{\rm CCW}a_{\rm CCW} + a^\dagger_{\rm CW}a_{\rm CW}) - i\hbar\frac{\gamma_m}{2}b^\dagger b. \tag{17}$$

Here, $\mathcal{H}$ is the Hamiltonian (1). The dissipations (κ, γ_m) of cavity and mechanical modes have been included to calculate the approximate solution of the probability amplitudes. Via setting $\partial|\psi\rangle/\partial t = 0$, a set of coupled linear equations for the coefficients $C_{n_{\rm CCW},n_{\rm CW},n_b}$ in the steady state can be obtained after straightforward calculation, with the forms

$$0 = \bar{\Delta}C_{1,0,0} + JC_{0,1,0} + gC_{1,0,1} + \varepsilon_L C_{0,0,0} + \sqrt{2}\varepsilon_L^* C_{2,0,0} + \varepsilon_R e^{i\theta}C_{1,1,0}, \tag{18}$$

$$0 = \bar{\Delta}C_{0,1,0} + JC_{1,0,0} + gC_{0,1,1} + \varepsilon_R e^{-i\theta}C_{0,0,0} + \varepsilon_L^* C_{1,1,0} + \sqrt{2}\varepsilon_R^* e^{i\theta}C_{0,2,0}, \tag{19}$$

$$0 = \bar{\Delta}C_{1,0,1} + JC_{0,1,1} + gC_{1,0,0} + \Omega_m C_{1,0,1} + \varepsilon_L C_{0,0,1}, \tag{20}$$

$$0 = \bar{\Delta}C_{0,1,1} + JC_{1,0,1} + gC_{0,1,0} + \Omega_m C_{0,1,1} + \varepsilon_R e^{-i\theta}C_{0,0,1}, \tag{21}$$

$$0 = 2\bar{\Delta}C_{1,1,0} + \sqrt{2}J(C_{2,0,0} + C_{0,2,0}) + \varepsilon_L C_{0,1,0} + \varepsilon_R e^{-i\theta}C_{1,0,0}, \tag{22}$$

$$0 = 2\bar{\Delta}C_{2,0,0} + \sqrt{2}JC_{1,1,0} + \sqrt{2}\varepsilon_L C_{1,0,0}, \tag{23}$$

$$0 = 2\bar{\Delta}C_{0,2,0} + \sqrt{2}JC_{1,1,0} + \sqrt{2}\varepsilon_R e^{-i\theta}C_{0,1,0}, \tag{24}$$

where $\bar{\Delta} = \Delta - i\frac{\kappa}{2}$ and $\Omega_m = \omega_m - i\frac{\gamma_m}{2}$. Within the weak driving limit, we take $C_{0,0,0} = 1$ [33,49]; two additional equations, namely, $\varepsilon_L^* C_{1,0,0} + \varepsilon_R^* e^{i\theta}C_{0,1,0} = 0$ and $\Omega_m C_{0,0,1} + \varepsilon_L^* C_{1,0,1} + \varepsilon_R^* e^{i\theta}C_{0,1,1} = 0$, are irrelevant to the problem [49]. Meanwhile, some subleading terms can also be neglected in Eqs. (18)–(24), for example, the terms $\sqrt{2}\varepsilon_L^* C_{2,0,0} + \varepsilon_R e^{i\theta}C_{1,1,0}$, $\varepsilon_L^* C_{1,1,0} + \sqrt{2}\varepsilon_R^* e^{i\theta}C_{0,2,0}$, $\varepsilon_L C_{0,0,1}$, as well as the term $\varepsilon_R e^{-i\theta}C_{0,0,1}$ [49]. With these simplifications, it is possible to obtain the analytical expressions of the coefficients $C_{n_{\rm CCW},n_{\rm CW},n_b}$ from Eqs. (18)–(24). Generally, the analytical expressions of $C_{n_{\rm CCW},n_{\rm CW},n_b}$ are complex. Combining Eqs. (13)–(15), the zero-time delay second-order correlation function $g^{(2)}_{a_{\rm CCW}}(0)$ in cavity mode CCW can be approximately yielded by [62]

$$g^{(2)}_{a_{\rm CCW}}(0) \approx \frac{2|C_{2,0,0}|^2}{|C_{1,0,0}|^4}. \tag{25}$$

Thus, for simplicity of calculation, only $C_{1,0,0}$ and $C_{2,0,0}$ are given as below:

$$C_{1,0,0} = \frac{(J\varepsilon_R e^{-i\theta} - \bar{\Delta}\varepsilon_L)B_1B_2 - g^2(J\varepsilon_R e^{-i\theta} + A\varepsilon_L)}{g^4 - 2g^2(J^2 + A\bar{\Delta}) + B_1B_2D_1D_2}, \tag{26}$$

$$C_{2,0,0} = \frac{J\varepsilon_R e^{-i\theta}(2\bar{\Delta}\varepsilon_L - J\varepsilon_R e^{-i\theta})E_1 + E_2\varepsilon_L^2}{-2\sqrt{2}\bar{\Delta}D_1D_2(B_1D_1 - g^2)(B_2D_2 - g^2)}, \tag{27}$$

where $A = \bar{\Delta} + \Omega_m$, $B_1 = J + A$, $B_2 = J - A$, $D_1 = J + \bar{\Delta}$, $D_2 = J - \bar{\Delta}$, $E_1 = 2\bar{\Delta}B_1B_2 + g^2\Omega_m$, and $E_2 = -2\bar{\Delta}^3B_1B_2 + g^2[(A + \bar{\Delta})D_1D_2 - \bar{\Delta}^2\Omega_m]$, respectively.

Based on Eqs. (25)–(27), the detailed analytical expression of the second-order correlation function $g^{(2)}_{a_{\rm CCW}}(0)$ can be achieved. Accordingly, the condition for $g^{(2)}_{a_{\rm CCW}}(0) \ll 1$ (i.e., $C_{2,0,0} \approx 0$) can also be calculated in the analytical form. However, the analytical expression of the second-order correlation function $g^{(2)}_{a_{\rm CCW}}(0)$ or the conditions for $g^{(2)}_{a_{\rm CCW}}(0) \ll 1$ (strong antibunching) is too cumbersome and is not presented here. But from the above expressions (26) and (27) it is quite obvious to show that the second-order correlation function $g^{(2)}_{a_{\rm CCW}}(0)$ is closely related to both the relative phase (θ) and the amplitudes (ε_L, ε_R) of the two driving fields. In the case that only one cavity mode is driven (namely, either the left-hand input field $\varepsilon_L = 0$ or the right-hand input field $\varepsilon_R = 0$), from Eqs. (26) and (27), we can see that the relative phase θ between them in the final analytical expression of the second-order correlation function $g^{(2)}_{a_{\rm CCW}}(0)$ disappears (i.e., phase independent) since we can eliminate it after the simple transformation. The relation between the photon statistics and the parameters ε_L or ε_R is considerably simple. Yet, in the case of the two cavity modes driven (both $\varepsilon_L \neq 0$ and $\varepsilon_R \neq 0$ simultaneously), it is clearly found from Eqs. (26) and (27) that the second-order correlation function $g^{(2)}_{a_{\rm CCW}}(0)$ becomes sensitive to the relative phase θ, because we cannot eliminate it. That is to say, optimal photon statistics is easy to be obtained by appropriately altering the control parameters θ, ε_L, and ε_R. It is pointed out that the leading role of introducing the two input driving fields is to induce the quantum interference between different transition pathways (see Fig. 4 below), which is necessary for phase-dependent effects in this system. With the system parameters experimentally used to study the photon statistics in the WGM microresonator optomechanical systems [53–56,65], the in-depth results of numerical calculation by the master-equation approach for different parameter conditions are presented in the following sections.

B. Case of only one cavity mode driven

In the work of Weis *et al.* [65] about OMIT, the circumstances that (i) only one CCW mode of the WGM microresonator is introduced and (ii) it is driven by an input field have been dealt with. For a better comparison in the present paper, we would like to explore the three-mode-coupling case where

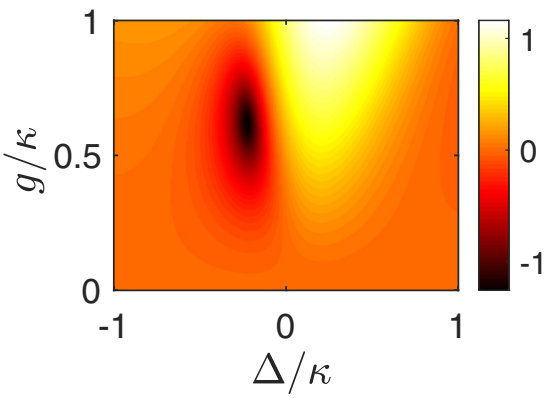

FIG. 3. Contour plot of the photon statistics spectrum in logarithmic scale $\log_{10}[g^{(2)}_{a_{\rm CCW}}(0)]$ of the cavity mode $a_{\rm CCW}$ plotted as a function of g/κ and Δ/κ when only the cavity mode $a_{\rm CCW}$ is driven by the input field $\varepsilon_L = 3\times10^{-3}\omega_m$. All other system parameters are given as $\varepsilon^R_{\rm in}=0$, $\bar{n}_{\rm th}=0$, $\kappa=0.1\omega_m$, $\gamma_m/\omega_m=10^{-4}$, $J=3\kappa$, and $\omega_m/2\pi=10$ MHz.

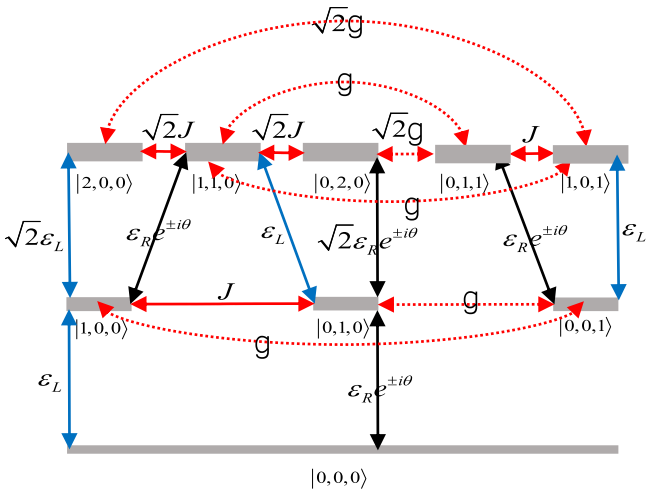

FIG. 4. Energy-level and transition path diagram of the coupled three-mode WGM microresonator optomechanical system. The quantum interference between different transition pathways for the two-photon state of the cavity mode $a_{\rm CCW}$ leads to the counterintuitive photon antibunching effect.

the CW and CCW modes are involved and one of them still is driven by an input field, but we are concerned about photon statistics. Without loss of generality, the right-hand input field is switched off, which is equivalent in Hamiltonian to $\varepsilon^R_{\rm in}=0$. Thus there is only the cavity mode $a_{\rm CCW}$ which is driven by the input field $\varepsilon^L_{\rm in}$. However, the other cavity mode $a_{\rm CW}$ can also be excited due to the mode coupling caused by the residual scattering of light from surface roughness or internal defect centers. Figure 3 plots the second-order correlation function $g^{(2)}_{a_{\rm CCW}}(0)$ of the cavity mode $a_{\rm CCW}$ in a logarithmic scale $\log_{10}[g^{(2)}_{a_{\rm CCW}}(0)]$ as a function of the optomechanical coupling strength g/κ and the detuning Δ/κ for the case of $\varepsilon^R_{\rm in}=0$. One can see that the cavity mode $a_{\rm CCW}$ can exhibit strong antibunching photon statistics in the black region with the negative detuning $\Delta<0$. Instead, there is only bunching or superbunching instead of antibunching for the positive detuning $\Delta>0$. Remarkably, the necessary condition for obtaining efficient antibunching photons is strong optomechanical coupling ($g>\kappa$) in the standard optomechanical system [58]. From Fig. 3, however, it is apparent that the antibunching photon statistics can be exhibited even in the weak optomechanical interaction regime. As we know, the single-photon regime is usually characterized by $g^{(2)}_{a_{\rm CCW}}(0)<0.5$ [41,72]. In Fig. 3, the strong antibunching, $\log_{10}[g^{(2)}_{a_{\rm CCW}}(0)]\approx-1.2$, can be found at $\Delta=0.22\kappa$ and $g=0.6\kappa$ together with the selected parameters. As a result, the preparation of the single-photon sources [$g^{(2)}_{a_{\rm CCW}}(0)$ is as low as 0.5] can be achieved by adjusting the system parameters in the weak optomechanical interaction regime.

The physical grounds for this pronounced antibunched photon statistics under the weak optomechanical coupling condition can be explained by the energy-level diagram of the coupled WGM microresonator optomechanical system (see Fig. 4). Different from the conventional blockade mechanism where the higher excitations are far off resonance due to the quantum anharmonicity ladder of the energy spectrum [13–15], this counterintuitive photon antibunching phenomenon is ascribed to the destructive quantum interference between different transition pathways for two-photon excitation. As is displayed in Fig. 4, multiple transition pathways can be used to achieve the excitation of the two-photon state for the cavity mode $a_{\rm CCW}$ when the condition of $\varepsilon^R_{\rm in}=0$ is satisfied. Among them, there is a direct transition pathway, $|0,0,0\rangle \xrightarrow{\varepsilon_L} |1,0,0\rangle \xrightarrow{\sqrt{2}\varepsilon_L} |2,0,0\rangle$, which is excited by the input field ε_L. In addition, the existence of the couplings (J and g) means that there are also some indirect pathways, for example, the pathways $|0,0,0\rangle \xrightarrow{\varepsilon_L} |1,0,0\rangle \xrightarrow{J} |0,1,0\rangle \xrightarrow{\varepsilon_L} |1,1,0\rangle \xrightarrow{\sqrt{2}J} |2,0,0\rangle$, $|0,0,0\rangle \xrightarrow{\varepsilon_L} |1,0,0\rangle \xrightarrow{g} |0,0,1\rangle \xrightarrow{\varepsilon_L} |1,0,1\rangle \xrightarrow{\sqrt{2}g} |2,0,0\rangle$, $|0,0,0\rangle \xrightarrow{\varepsilon_L} |1,0,0\rangle \xrightarrow{J} |0,1,0\rangle \xrightarrow{g} |0,0,1\rangle \xrightarrow{\varepsilon_L} |1,0,1\rangle \xrightarrow{\sqrt{2}g} |2,0,0\rangle$, and so on. The direct transition pathway for the two-photon excitation may be forbidden by the destructive quantum interference with the other indirect pathways. In other words, the destructive quantum interference between the direct transition pathway and the indirect pathways or the interference between the indirect transition pathways can reduce the probability in the two-photon excited state. The above results are based on the weak optomechanical coupling condition. This means that the mode coupling J plays a crucial role in the pathway interference.

From the above analysis, for the case that only the cavity mode $a_{\rm CCW}$ is driven by the input field $\varepsilon^L_{\rm in}$, we can conclude that this counterintuitive antibunching photon statistics under the weak optomechanical coupling condition results from the destructive quantum interference between the different transition pathways for the two-photon excited state. Different from the conventional photon blockade in a strongly nonlinear system [13–18], the interference-based photon antibunching is also referred to as an unconventional photon blockade. Because the master equation (1) shows that the physical properties of the cavity modes $a_{\rm CCW}$ and $a_{\rm CW}$ are equivalent, photon statistical properties of the cavity mode $a_{\rm CW}$ can also be studied in a similar way.

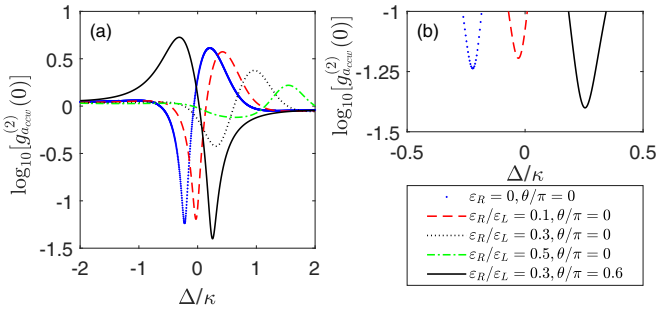

FIG. 5. (a) The photon statistics spectrum in logarithmic scale $\log_{10}[g^{(2)}_{a_{CCW}}(0)]$ of the cavity mode a_{CCW} varying with the detuning Δ/κ for the case that the two cavity modes are simultaneously driven. Blue starred line, $\varepsilon_L = 3\times10^{-3}\omega_m$, $\varepsilon_R = 0$, and $\theta/\pi = 0$; red dashed line, $\varepsilon_L = 3\times10^{-3}\omega_m$, $\varepsilon_R = 0.1\varepsilon_L$, and $\theta = 0$; black dotted line, $\varepsilon_L = 3\times10^{-3}\omega_m$, $\varepsilon_R = 0.3\varepsilon_L$, and $\theta = 0$; green dot-dashed line, $\varepsilon_L = 3\times10^{-3}\omega_m$, $\varepsilon_R = 0.5\varepsilon_L$, and $\theta = 0$; black solid line, $\varepsilon_L = 3\times10^{-3}\omega_m$, $\varepsilon_R = 0.3\varepsilon_L$, and $\theta/\pi = 0.6$. (b) Partially enlarged view of the photon statistics spectrum in (a). All other system parameters are given as $\bar{n}_{th} = 0$, $\gamma_m/\omega_m = 10^{-4}$, $\kappa = 0.1\omega_m$, $J = 3\kappa$, $g = 0.6\kappa$, and $\omega_m/2\pi = 10$ MHz.

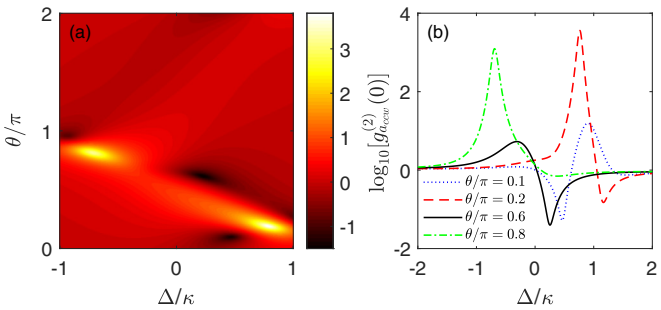

FIG. 6. (a) Contour plot of the photon statistics spectrum in logarithmic scale $\log_{10}[g^{(2)}_{a_{CCW}}(0)]$ of the cavity mode a_{CCW} plotted as a function of the relative phase θ/π and the detuning Δ/κ under the weak optomechanical coupling regime. (b) The photon statistics spectrum in logarithmic scale $\log_{10}[g^{(2)}_{a_{CCW}}(0)]$ of the cavity mode a_{CCW} varying with the detuning Δ/κ under different phases θ: $\theta/\pi = 0.1$ (blue dotted line), $\theta/\pi = 0.2$ (red dashed line), $\theta/\pi = 0.6$ (black solid line), and $\theta/\pi = 0.8$ (green dot-dashed line). The WGM microresonator optomechanical system is driven by the two input fields $\varepsilon_L = 3\times10^{-3}\omega_m$ and $\varepsilon_R = 0.3\varepsilon_L$ at the same time. All other system parameters are given as $\bar{n}_{th} = 0$, $\gamma_m/\omega_m = 10^{-4}$, $\kappa = 0.1\omega_m$, $J = 3\kappa$, $g = 0.6\kappa$, and $\omega_m/2\pi = 10$ MHz.

C. Case of two cavity modes simultaneously driven

In the previous subsection, for the case that only one cavity mode is driven by the input field, the interference-based photon antibunching can be exhibited under the weak optomechanical coupling condition. This phenomenon appears because the other cavity mode can also be excited when the mode coupling takes place between the counterpropagating cavity modes. Logically, an interesting question is what happens when the other cavity mode is also driven by an additional input field, not just by the residual scattering of light. As the extra input field can provide more freedom to adjust the quantum interference between different transition pathways, more colorful photon statistical phenomena can be observed. In this part, we thus extend our studies to the case where the CW and CCW cavity modes are simultaneously driven by two separated input fields, namely, $\varepsilon^L_{in} \neq 0$ and $\varepsilon^R_{in} \neq 0$. Accordingly, a relative phase θ between the left-hand and right-hand input fields on both ports needs to be established. First, for a fixed ε_L, we present a discussion on the influence of the amplitude ε_R on the photon statistical properties of the system. Then, we mainly focus on the effect of the relative phase θ between the left-hand and right-hand input fields on the photon statistical properties. To keep the parameters consistent, all of the results are under the weak-coupling condition $g = 0.6\kappa$. The detailed results are given in Figs. 5 and 6.

For the sake of better comparison, we fix $\varepsilon_L = 3\times10^{-3}\omega_m$ in the following discussion. Figure 5(a) displays the second-order correlation function in a logarithmic scale $\log_{10}[g^{(2)}_{a_{CCW}}(0)]$ varying with the detuning Δ/κ when both left-hand input field ε^L_{in} and right-hand input field ε^R_{in} are applied at the same time. In order to investigate the influence of the amplitudes on the photon statistic properties, by fixing the value of the relative phase between the left-hand and right-hand fields to be $\theta = 0$, we change the value of ε_R from 0 to $0.5\varepsilon_L$. In the case of $\varepsilon_R = 0$, as is plotted with the starred line in Fig. 5(a), the profile of the second-order correlation function in a logarithmic scale $\log_{10}[g^{(2)}_{a_{CCW}}(0)]$ varying with the detuning Δ/κ exhibits a dip-peak structure. With the increasing of the detuning Δ, the value of $\log_{10}[g^{(2)}_{a_{CCW}}(0)]$ first arrives at the minimum (dip) and then at the maximum (peak). Moreover, its minimum value is about -1.24 at the dip, and its maximum value is about 0.61 at the peak. It is apparent that the strong antibunching photon statistics can be produced at the dip. When $\varepsilon_R = 0.1\varepsilon_L$, as is described by the red dashed line, it can be found from the profile that the second-order correlation function in a logarithmic scale $\log_{10}[g^{(2)}_{a_{CCW}}(0)]$ still displays dip-peak structure, with its minimum value at about -1.19. Furthermore, the curves of $\log_{10}[g^{(2)}_{a_{CCW}}(0)]$ are plotted for the cases of $\varepsilon^R_{in} = 0.3\varepsilon_L$ and $0.5\varepsilon_L$. Finally, the black dotted line gives the profile for the case of $\varepsilon^R_{in} = 0.3\varepsilon_L$ and the green dot-dashed line corresponds to the profile of $\varepsilon^R_{in} = 0.5\varepsilon_L$ in Fig. 5(a). The minimum values of $\log_{10}[g^{(2)}_{a_{CCW}}(0)]$ for the cases of $\varepsilon^R_{in} = 0.3\varepsilon_L$ and $0.5\varepsilon_L$ are -0.42 and -0.12, respectively.

It is well known that photon antibunching occurs when the value of the second-order correlation function $g^{(2)}_{a_{CCW}}(0)$ in a logarithmic scale $\log_{10}[g^{(2)}_{a_{CCW}}(0)]$ is negative. Moreover, the smaller the value of the second-order correlation function $g^{(2)}_{a_{CCW}}(0)$ in a logarithmic scale is, the stronger the photon antibunching effect is. Interestingly, according to the above discussions, the minimum values of the second-order correlation function $g^{(2)}_{a_{CCW}}(0)$ in a logarithmic scale $\log_{10}[g^{(2)}_{a_{CCW}}(0)]$ can get bigger and bigger with gradual increasing of the amplitude of ε^R_{in}. So we can summarize from the obtained results that when both cavity modes are driven at the same time the optimal photon antibunching is weakened instead of enhanced with the increase of the amplitude ε_R. Physically, this may be because some additional transition pathways can be introduced to achieve the excitation of the two-photon state of the cavity mode a_{CCW} with the help of the couplings J and g when the cavity mode a_{CW} is also driven by the additional input field ε^R_{in}.

The case that the relative phase of $\theta \neq 0$ seems to be more nontrivial. Actually, a relative phase θ between the left-hand and right-hand input fields can be established when both cavity modes are driven at the same time. It is necessary to take the relative phase θ into account in our analysis. It can be clearly seen from the black solid line in Fig. 5(a) that, for a given amplitude $\varepsilon_R = 0.3\varepsilon_L$ and phase $\theta/\pi = 0.6$, the profile of the second-order correlation function $g^{(2)}_{a_{\rm CCW}}(0)$ in a logarithmic scale $\log_{10}[g^{(2)}_{a_{\rm CCW}}(0)]$ takes on a clear peak-dip structure. Compared to the black dotted line where $\theta/\pi = 0$ in Fig. 5(a), the depth of the antibunching dip considerably deepens, which indicates the photon antibunching is significantly enhanced. Interestingly, its minimum value can be even smaller than that of the optimized case when $\varepsilon_R = 0$, i.e., the blue starred line for $\theta = 0$ in Fig. 5(a). Figure 5(b) is the partially enlarged view of the photon statistics spectrum in Fig. 5(a). It indirectly indicates that, compared to the case of only one cavity mode driven, the photon antibunching can be enhanced by appropriately adjusting the relative phase θ when the two cavity modes are simultaneously driven. Combining Figs. 5(a) and 5(b), we arrive at an important conclusion that the antibunching photon statistics can be manipulated and optimized by means of the relative phase θ for the case that the two cavity modes are simultaneously driven. A similar method can also be used to discuss the bunching peak of the second-order correlation function $g^{(2)}_{a_{\rm CCW}}(0)$.

In order to further illustrate explicitly the role of the relative phase θ in the photon statistical properties. In Fig. 6(a), we plot the second-order correlation function $g^{(2)}_{a_{\rm CCW}}(0)$ of the cavity mode $a_{\rm CCW}$ in a logarithmic scale $\log_{10}[g^{(2)}_{a_{\rm CCW}}(0)]$ as a function of the relative phase θ/π and the detuning Δ/κ under the weak optomechanical coupling regime $g = 0.6\kappa$. What should be emphasized is that the two cavity modes of the WGM microresonator are separately driven by the input fields $\varepsilon^L_{\rm in}$ and $\varepsilon^R_{\rm in}$ at the same time. Meanwhile, the amplitudes of the left-hand and right-hand input fields are fixed to $\varepsilon_L = 3 \times 10^{-3}\omega_m$ and $\varepsilon_R = 0.3\varepsilon_L$, respectively. Generally speaking, the values of $\log_{10}[g^{(2)}_{a_{\rm CCW}}(0)] < 0$ refer to photon antibunching, which corresponds to sub-Poissonian photon statistics, and the probability to excite the two-photon state is smaller than that to excite two single-photon states independently. For the case of $\log_{10}[g^{(2)}_{a_{\rm CCW}}(0)] > 0$, photons inside the cavity enhance the resonantly entering probability of subsequent photons. Then under certain conditions, photon-induced tunneling occurs [62], namely, super-Poissonian photon statistics occurs. As is clearly displayed in Fig. 6(a), the distribution of photons in the cavity mode $a_{\rm CCW}$ can be observed, which is phase dependent when the two cavity modes are coherently driven at the same time. One can see, whether in the red-detuning regime $\Delta > 0$ or in the blue-detuning regime $\Delta < 0$, that both antibunching and superbunching phenomena can be realized in cavity mode $a_{\rm CCW}$ by properly tuning the relative phase θ between the left-hand and right-hand input fields. For example, for $\Delta \approx 0.23\kappa$ in the red-detuning regime, the value of $\log_{10}[g^{(2)}_{a_{\rm CCW}}(0)]$ can arrive at -1.5 when the relative phase $\theta/\pi \approx 0.61$. This means that the cavity mode $a_{\rm CCW}$ can exhibit a strong antibunching photon statistics at this point. With the same value of θ, however, the cavity mode $a_{\rm CCW}$ indicates super-Poissonian photon statistics instead of antibunching in the blue-detuning regime. Note that the photon antibunching can be achieved by adjusting the relative phase between the left-hand and right-hand input fields to be $\theta/\pi \approx 1.3$ for $\Delta \approx -0.23\kappa$. With the increase of the detuning Δ, the antibunching and superbunching photon statistics can be observed by adjusting the relative phase θ. This proves that the resulting photon statistics of the cavity field $a_{\rm CCW}$ indeed is affected by the relative phase θ, where the strong photon antibunching can be generated by choosing the proper phase θ.

Next, in Fig. 6(b), the second-order correlation function in a logarithmic scale $\log_{10}[g^{(2)}_{a_{\rm CCW}}(0)]$ is plotted as a function of the detuning Δ/κ under four different relative phases θ, namely, $\theta/\pi = 0.1$ (blue dotted line), $\theta/\pi = 0.2$ (red dashed line), $\theta/\pi = 0.6$ (black solid line), and $\theta/\pi = 0.8$ (green dot-dashed line). The maximum (peak) values for the $\log_{10}[g^{(2)}_{a_{\rm CCW}}(0)]$ curves of $\theta/\pi = 0.1$, 0.2, 0.6, and 0.8 are 1.19, 3.56, 0.73, and 3.10, respectively. Meanwhile, their minimum (dip) values of $\log_{10}[g^{(2)}_{a_{\rm CCW}}(0)]$ are -1.28, -0.82, -1.40, and -0.15, respectively. From this figure, it is obvious that the tendencies of the maximum values and minimum values for $\log_{10}[g^{(2)}_{a_{\rm CCW}}(0)]$ do not change monotonously with the relative phase θ. This suggests that optimal superbunching and antibunching can be achieved when properly choosing θ. That is also to say, by carefully varying the value of θ, it is possible to find the positions for the strongest superbunching and antibunching.

In the case that only one optical cavity mode is driven by the input field, the other cavity mode can also be driven by the residual scattering of light owing to mode coupling. In the case that both optical cavity modes are driven at the same time, though extra amplitude and relative phase are added, the antibunching may be also interpreted with similar physics processes as shown in Fig. 4. Because the cavity mode $a_{\rm CW}$ is also driven by the input field ε_R, some additional transition pathways are introduced to achieve the excitation of the two-photon state. Additionally, these transition pathways are phase dependent; for instance, the pathways $|0,0,0\rangle \xrightarrow{\varepsilon_L} |1,0,0\rangle \xrightarrow{\varepsilon_R e^{\pm i\theta}} |1,1,0\rangle \xrightarrow{\sqrt{2}J} |2,0,0\rangle$, $|0,0,0\rangle \xrightarrow{\varepsilon_R e^{\pm i\theta}} |0,1,0\rangle \xrightarrow{\sqrt{2}\varepsilon_R e^{\pm i\theta}} |0,2,0\rangle \xrightarrow{\sqrt{2}J} |1,1,0\rangle \xrightarrow{\sqrt{2}J} |2,0,0\rangle$, and $|0,0,0\rangle \xrightarrow{\varepsilon_L} |1,0,0\rangle \xrightarrow{g} |0,0,1\rangle \xrightarrow{\varepsilon_R e^{\pm i\theta}} |0,1,1\rangle \xrightarrow{g} |1,1,0\rangle \xrightarrow{\sqrt{2}J} |2,0,0\rangle$ can all be affected by the relative phase θ between the left-hand and right-hand input fields. Because the phase is adjustable, the destructive quantum interference between these extra transition paths and the original transition paths is manageable. Accordingly, the photon antibunching can be modulated and optimized by the relative phase θ between the two input fields.

In all of the above discussions, our attention has been focused on the situation of the thermal phonon number $\bar{n}_{\rm th} = 0$, i.e., we have ignored the effect of the environment thermal phonon number on the photon statistical properties. However, the system can inevitably interact with the environment. This means that the effect of the thermal noise on the photon statistical properties should be included. In Fig. 7, the second-order correlation function in a logarithmic scale $\log_{10}[g^{(2)}_{a_{\rm CCW}}(0)]$ is plotted as a function of the detuning Δ/κ under different mean thermal phonon numbers $\bar{n}_{\rm th}$ for the cases of $\theta/\pi = 0.2$ and 0.6. Clearly, with the decrease of the mean thermal phonon numbers $\bar{n}_{\rm th}$, the peak (maximum) of the second-order correlation function in a logarithmic scale $\log_{10}[g^{(2)}_{a_{\rm CCW}}(0)]$ becomes higher and higher in Fig. 7(a), while the dip (minimum) of

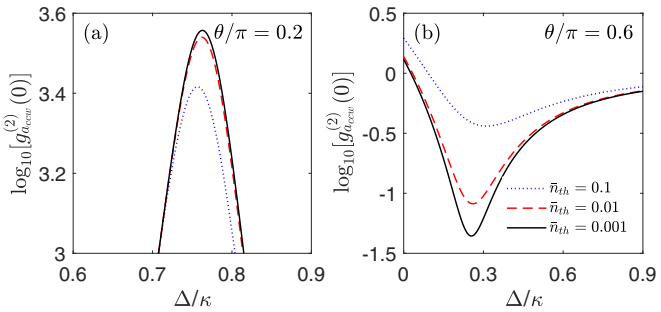

FIG. 7. The photon statistics spectrum in logarithmic scale $\log_{10}[g^{(2)}_{a_{\rm CCW}}(0)]$ of the cavity mode $a_{\rm CCW}$ as a function of the detuning Δ/κ under different mean thermal phonon number $\bar{n}_{\rm th}$ (blue dotted curve for $\bar{n}_{\rm th} = 0.1$, red dashed curve for $\bar{n}_{\rm th} = 0.01$, and black solid curve for $\bar{n}_{\rm th} = 0.001$). (a) $\theta/\pi = 0.2$. (b) $\theta/\pi = 0.6$. All other system parameters are given as $\varepsilon_L = 3 \times 10^{-3}\omega_m$, $\varepsilon_R = 0.3\varepsilon_L$, $\gamma_m/\omega_m = 10^{-4}$, $\kappa = 0.1\omega_m$, $J = 3\kappa$, $g = 0.6\kappa$, and $\omega_m/2\pi = 10$ MHz.

the $\log_{10}[g^{(2)}_{a_{\rm CCW}}(0)]$ in Fig. 7(b) is deeper and deeper. These numerical results show that the environment phonon numbers have an undesirable effect on the realization of the strong antibunching and superbunching photon statistics. Therefore it is necessary to prepare the mechanical resonator near to the ground state to overcome the undesirable effect induced by the environmentally thermal phonons.

V. DISCUSSIONS AND CONCLUSIONS

The latent applications of strong photon antibunching in quantum information and quantum optics fields have attracted wide interest. For its practical applications, however, parameter tunable photon antibunching is usually expected. As an example, the single-photon source is one of the most important applications of strong photon antibunching. The parameter tunable single-photon source can help us to understand the impact of photon number on the security of quantum information [73]. Yet, for general optical cavities, it is not easy to realize experimentally due to the original form of the model where only one of the optical cavity modes is driven by the input field [36,37]. This is because it requires a fine tuning of the intrinsic system parameters, as the optimal photon antibunching can be obtained for proper interrelations between the laser detuning, the cavity coupling, and the nonlinearity [36,37,40,41,49]. For the case that only one optical cavity mode is driven by the input field, the system dynamics is phase independent and the parameters used to adjust the photon antibunching are limited. For the case of two cavity modes simultaneously driven, the system is sensitive to the relative phase between them. The parameter constraints for strong photon antibunching can be naturally absorbed in the amplitude and the relative phase between the two input fields [40,41]. As we know, the phase is an adjustable parameter, which can be controlled precisely in experiments, e.g., by using piezoelectric transducers [74]. Thus, the statistical properties of photons can be modulated and optimized by regulating the relative phase between the two input fields. As a consequence, compared to the case of only one cavity mode driven, one can achieve a stronger photon antibunching or superbunching associated with a well-behaved zero-time delay second-order correlation function for a wider range of system parameters when the two cavity modes are simultaneously driven.

In summary, we have studied the photon statistical properties in a three-mode-coupling WGM microresonator optomechanical system. It is revealed that the mode coupling between the CW and CCW modes, which is usually caused by the scattering of light due to surface roughness or internal defect centers, plays an important role in controlling the output power spectra of the WGM microresonator. What is more, because of the mode coupling, destructive interferences between different transition pathways can occur. By solving numerically the quantum master equation, the results display that strong photon antibunching statistics can be generated when only one cavity mode is driven by the input field, even for the weak optomechanical coupling condition. On the other hand, we have focused our interest mainly on the case that the two cavity modes of the WGM microresonator are driven by two separated input fields at the same time. We analyze in depth the influences of the amplitude, and especially the relative phase between the two input fields on the photon statistical properties of the system. It is shown that more transition pathways can be provided for the coupled system to be excited from the ground state to the two-photon state when both cavity modes are driven by the two input fields, compared with those where only one cavity mode is driven. Moreover, the transition paths for the latter can be modulated by the relative phase between the two input fields, which in turn modifies the photon statistical properties of the cavity mode. We demonstrate that the second-order correlation function of the cavity mode does not vary monotonously with the value of the relative phase between the two input fields. Thus the photon statistic properties can be optimized by properly adjusting the value of the relative phase. Finally, it is demonstrated that the thermal noise has detrimental effect on the photon statistical properties. Because these photon statistical phenomena are observed in the weak optomechanical coupling regime, the parameters chosen in our numerical simulations are experimentally possible. The proposed scheme may have latent applications for steering photon statistical properties with the present technology.

ACKNOWLEDGMENTS

We gratefully acknowledge the referees for helpful criticism and questions. Their careful and in-depth review enriched our paper. We also acknowledge the helpful discussions with Prof. Xiaoxue Yang and Dr. Rong Yu during the manuscript preparation and acknowledge contributions to the numerical simulations by Dr. Zihao Li. Both Y.Q. and J.L. are supported in part by the National Natural Science Foundation of China under Grant No. 11675058 and the Fundamental Research Funds for the Central Universities (Huazhong University of Science and Technology) under Grant No. 2018KFYYXJJ037. Y.W. is supported in part by the National Key Research and Development Program of China under Grant No. 2016YFA0301200 as well as the National Natural Science Foundation of China under Grants No. 11875029 and No. 11574104.

[1] T. Peyronel, O. Firstenberg, Q. Y. Liang, S. Hofferberth, A. V. Gorshkov, T. Pohl, M. D. Lukin, and V. Vuletić, Quantum nonlinear optics with single photons enabled by strongly interacting atoms, Nature (London) **488**, 57 (2012).

[2] S. Ferretti, V. Savona, and D. Gerace, Optimal antibunching in passive photonic devices based on coupled nonlinear resonators, New J. Phys. **15**, 025012 (2013).

[3] V. Giovannetti, S. Lloyd, and L. Maccone, Quantum Metrology, Phys. Rev. Lett. **96**, 010401 (2006).

[4] E. Knill, R. Laflamme, and G. J. Milburn, A scheme for efficient quantum computation with linear optics, Nature (London) **409**, 46 (2001).

[5] T. Jennewein, M. Barbieri, and A. G. White, Single-photon device requirements for operating linear optics quantum computing outside the post-selection basis, J. Mod. Opt. **58**, 276 (2011).

[6] I. Buluta and F. Nori, Quantum simulators, Science **326**, 108 (2009).

[7] I. M. Georgescu, S. Ashhab, and F. Nori, Quantum simulation, Rev. Mod. Phys. **86**, 153 (2014).

[8] J. L. O'Brien, A. Furusawa, and J. Vučković, Photonic quantum technologies, Nat. Photonics **3**, 687 (2009).

[9] V. Scarani, H. Bechmann-Pasquinucci, N. J. Cerf, M. Dušek, N. Lütkenhaus, and M. Peev, The security of practical quantum key distribution, Rev. Mod. Phys. **81**, 1301 (2009).

[10] T. A. Fulton and G. J. Dolan, Observation of Single-Electron Charging Effects in Small Tunnel Junctions, Phys. Rev. Lett. **59**, 109 (1987).

[11] M. A. Kastner, The single-electron transistor, Rev. Mod. Phys. **64**, 849 (1992).

[12] K. K. Likharev, Single-electron devices and their applications, Proc. IEEE **87**, 606 (1999).

[13] A. Imamoğlu, H. Schmidt, G. Woods, and M. Deutsch, Strongly Interacting Photons in a Nonlinear Cavity, Phys. Rev. Lett. **79**, 1467 (1997).

[14] M. J. Werner and A. Imamoğlu, Photon-photon interactions in cavity electromagnetically induced transparency, Phys. Rev. A. **61**, 011801(R) (1999).

[15] R. J. Brecha, P. R. Rice, and M. Xiao, N two-level atoms in a driven optical cavity: Quantum dynamics of forward photon scattering for weak incident fields, Phys. Rev. A. **59**, 2392 (1999).

[16] S. Rebić, A. S. Parkins, and S. M. Tan, Polariton analysis of a four-level atom strongly coupled to a cavity mode, Phys. Rev. A. **65**, 043806 (2002).

[17] S. Rebić, A. S. Parkins, and S. M. Tan, Photon statistics of a single-atom intracavity system involving electromagnetically induced transparency, Phys. Rev. A. **65**, 063804 (2002).

[18] K. M. Birnbaum, A. Boca, R. Miller, A. D. Boozer, T. E. Northup, and H. J. Kimble, Photon blockade in an optical cavity with one trapped atom, Nature (London) **436**, 87 (2005).

[19] A. Miranowicz, M. Paprzycka, Y. X. Liu, J. Bajer, and F. Nori, Two-photon and three-photon blockades in driven nonlinear systems, Phys. Rev. A. **87**, 023809 (2013).

[20] Y. X. Liu, X. W. Xu, A. Miranowicz, and F. Nori, From blockade to transparency: Controllable photon transmission through a circuit-QED system, Phys. Rev. A. **89**, 043818 (2014).

[21] W. W. Deng, G. X. Li, and H. Qin, Enhancement of the two-photon blockade in a strong-coupling qubit-cavity system, Phys. Rev. A. **91**, 043831 (2015).

[22] M. Bradford and J. T. Shen, Architecture dependence of photon antibunching in cavity quantum electrodynamics, Phys. Rev. A. **92**, 023810 (2015).

[23] K. Müller, A. Rundquist, K. A. Fischer, T. Sarmiento, K. G. Lagoudakis, Y. A. Kelaita, C. S. Muñoz, E. del Valle, F. P. Laussy, and J. Vučković, Coherent Generation of Nonclassical Light on Chip Via Detuned Photon Blockade, Phys. Rev. Lett. **114**, 233601 (2015).

[24] M. J. Hartmann, F. G. S. L. Brandão, and M. B. Plenio, Strongly interacting polaritons in coupled arrays of cavities, Nat. Phys. **2**, 849 (2006).

[25] D. E. Chang, V. Gritsev, G. Morigi, V. Vuletić, M. D. Lukin, and E. A. Demler, Crystallization of strongly interacting photons in a nonlinear optical fibre, Nat. Phys. **4**, 884 (2008).

[26] B. Dayan, A. S. Parkins, T. Aoki, E. P. Ostby, K. J. Vahala, and H. J. Kimble, A photon turnstile dynamically regulated by one atom, Science **319**, 1062 (2008).

[27] A. Faraon, I. Fushman, D. Englund, N. Stoltz, P. Petroff, and J. Vučković, Coherent generation of non-classical light on a chip via photon-induced tunnelling and blockade, Nat. Phys. **4**, 859 (2008).

[28] J. M. Fink, M. Göppl, M. Baur, R. Bianchetti, P. J. Leek, A. Blais, and A. Wallraff, Climbing the Jaynes-Cummings ladder and observing its nonlinearity in a cavity QED system, Nature (London) **454**, 315 (2008).

[29] F. Dubin, C. Russo, H. G. Barros, A. Stute, C. Becher, P. O. Schmidt, and R. Blatt, Quantum to classical transition in a single-ion laser, Nat. Phys. **6**, 350 (2010).

[30] E. Illes and S. Hughes, Photon antibunching in strongly coupled exciton-semiconductor cavity systems: Role of off-resonant coupling to multiple excitons, Phys. Rev. B. **81**, 121310(R) (2010).

[31] W. Zhang, Z. Y. Yu, Y. M. Liu, and Y. W. Peng, Optimal photon antibunching in a quantum-dot-bimodal-cavity system, Phys. Rev. A. **89**, 043832 (2014).

[32] A. Miranowicz, J. Bajer, M. Paprzycka, Y. X. Liu, A. M. Zagoskin, and F. Nori, State-dependent photon blockade via quantum-reservoir engineering, Phys. Rev. A. **90**, 033831 (2014).

[33] Y. L. Liu, G. Z. Wang, Y. X. Liu, and F. Nori, Mode coupling and photon antibunching in a bimodal cavity containing a dipole quantum emitter, Phys. Rev. A. **93**, 013856 (2016).

[34] C. Lang, D. Bozyigit, C. Eichler, L. Steffen, J. M. Fink, A. A. Abdumalikov Jr., M. Baur, S. Filipp, M. P. da Silva, A. Blais, and A. Wallraff, Observation of Resonant Photon Blockade at Microwave Frequencies Using Correlation Function Measurements, Phys. Rev. Lett. **106**, 243601 (2011).

[35] A. J. Hoffman, S. J. Srinivasan, S. Schmidt, L. Spietz, J. Aumentado, H. E. Türeci, and A. A. Houck, Dispersive Photon Blockade in a Superconducting Circuit, Phys. Rev. Lett. **107**, 053602 (2011).

[36] T. C. H. Liew and V. Savona, Single Photons From Coupled Quantum Modes, Phys. Rev. Lett. **104**, 183601 (2010).

[37] M. Bamba, A. Imamoğlu, I. Carusotto, and C. Ciuti, Origin of strong photon antibunching in weakly nonlinear photonic molecules, Phys. Rev. A. **83**, 021802(R) (2011).

[38] A. Majumdar, M. Bajcsy, A. Rundquist, and J. Vučković, Loss-Enabled Sub-Poissonian Light Generation in a Bimodal Nanocavity, Phys. Rev. Lett. **108**, 183601 (2012).

[39] H. Flayac and V. Savona, Input-output theory of the unconventional photon blockade, Phys. Rev. A. **88**, 033836 (2013).

[40] X. W. Xu and Y. Li, Tunable photon statistics in weakly nonlinear photonic molecules, Phys. Rev. A. **90**, 043822 (2014).

[41] H. Flayac and V. Savona, Unconventional photon blockade, Phys. Rev. A. **96**, 053810 (2017).

[42] D. Gerace and V. Savona, Unconventional photon blockade in doubly resonant microcavities with second-order nonlinearity, Phys. Rev. A. **89**, 031803(R) (2014).

[43] Y. H. Zhou, H. Z. Shen, and X. X. Yi, Unconventional photon blockade with second-order nonlinearity, Phys. Rev. A. **92**, 023838 (2015).

[44] H. Flayac and V. Savona, Single photons from dissipation in coupled cavities, Phys. Rev. A. **94**, 013815 (2016).

[45] M. A. Lemonde, N. Didier, and A. A. Clerk, Antibunching and unconventional photon blockade with Gaussian squeezed states, Phys. Rev. A. **90**, 063824 (2014).

[46] X. W. Xu and Y. Li, Strong photon antibunching of symmetric and antisymmetric modes in weakly nonlinear photonic molecules, Phys. Rev. A. **90**, 033809 (2014).

[47] J. Tang, W. Geng, and X. Xu, Quantum interference induced photon blockade in a coupled single quantum dot-cavity system, Sci. Rep. **5**, 9252 (2015).

[48] X.-W. Xu and Y.-J. Li, Antibunching photons in a cavity coupled to an optomechanical system, J. Phys. B **46**, 035502 (2013).

[49] V. Savona, Unconventional photon blockade in coupled optomechanical systems, arXiv:1302.5937v2.

[50] J. H. Li and Y. Wu, Quality of photon antibunching in two cavity-waveguide arrangements on a chip, Phys. Rev. A. **98**, 053801 (2018).

[51] C. Vaneph, A. Morvan, G. Aiello, M. Féchant, M. Aprili, J. Gabelli, and J. Estève, Observation of the Unconventional Photon Blockade in the Microwave Domain, Phys. Rev. Lett. **121**, 043602 (2018).

[52] H. J. Snijders, J. A. Frey, J. Norman, H. Flayac, V. Savona, A. C. Gossard, J. E. Bowers, M. P. van Exter, D. Bouwmeester, and W. Löffler, Observation of the Unconventional Photon Blockade, Phys. Rev. Lett. **121**, 043601 (2018).

[53] T. J. Kippenberg and K. J. Vahala, Cavity optomechanics: Back-action at the mesoscale, Science **321**, 1172 (2008).

[54] F. Marquardt and S. M. Girvin, Trend: Optomechanics, Physics **2**, 40 (2009).

[55] M. Aspelmeyer, P. Meystre, and K. Schwab, Quantum optomechanics, Phys. Today **65**(7), 29 (2012).

[56] M. Aspelmeyer, T. J. Kippenberg, and F. Marquardt, Cavity optomechanics, Rev. Mod. Phys. **86**, 1391 (2014).

[57] M. Metcalfe, Applications of cavity optomechanics, Appl. Phys. Rev. **1**, 031105 (2014).

[58] P. Rabl, Photon Blockade Effect in Optomechanical Systems, Phys. Rev. Lett. **107**, 063601 (2011).

[59] A. Nunnenkamp, K. Børkje, and S. M. Girvin, Single-Photon Optomechanics, Phys. Rev. Lett. **107**, 063602 (2011).

[60] J. Q. Liao and C. K. Law, Correlated two-photon scattering in cavity optomechanics, Phys. Rev. A. **87**, 043809 (2013).

[61] J. Q. Liao and F. Nori, Photon blockade in quadratically coupled optomechanical systems, Phys. Rev. A. **88**, 023853 (2013).

[62] X. W. Xu, Y. J. Li, and Y. X. Liu, Photon-induced tunneling in optomechanical systems, Phys. Rev. A. **87**, 025803 (2013).

[63] X. Y. Lü, Y. Wu, J. R. Johansson, H. Jing, J. Zhang, and F. Nori, Squeezed Optomechanics with Phase-Matched Amplification and Dissipation, Phys. Rev. Lett. **114**, 093602 (2015).

[64] C. Q. Wang, Y. L. Liu, R. B. Wu, and Y. X. Liu, Phase-modulated photon antibunching in a two-level system coupled to two cavities, Phys. Rev. A. **96**, 013818 (2017).

[65] S. Weis, R. Rivière, S. Deléglise, E. Gavartin, O. Arcizet, A. Schliesser, and T. J. Kippenberg, Optomechanically induced transparency, Science **330**, 1520 (2010).

[66] H. Lü, C. Q. Wang, L. Yang, and H. Jing, Optomechanically Induced Transparency at Exceptional Points, Phys. Rev. Appl. **10**, 014006 (2018).

[67] W. J. Chen, Ş. K. Özdemir, G. M. Zhao, J. Wiersig, and L. Yang, Exceptional points enhance sensing in an optical microcavity, Nature (London) **548**, 192 (2017).

[68] L. Allen and J. H. Eberly, *Optical Resonance and Two-Level Atoms* (Dover, New York, 1987).

[69] M. J. Collett and C. W. Gardiner, Squeezing of intracavity and traveling-wave light fields produced in parametric amplification, Phys. Rev. A. **30**, 1386 (1984).

[70] C. W. Gardiner and M. J. Collett, Input and output in damped quantum systems: Quantum stochastic differential equations and the master equation, Phys. Rev. A. **31**, 3761 (1985).

[71] H. J. Carmichael, *An Open Systems Approach to Quantum Optics*, Lecture Notes in Physics Vol. 18 (Spinger-Verlag, Berlin, 1993).

[72] J. Gallego, W. Alt, T. Macha, M. M. Dorantes, D. Pandey, and D. Meschede, Strong Purcell Effect on a Neutral Atom Trapped in an Open Fiber Cavity, Phys. Rev. Lett. **121**, 173603 (2018).

[73] N. Gisin, G. Ribordy, W. Tittel, and H. Zbinden, Quantum cryptography, Rev. Mod. Phys. **74**, 145 (2002).

[74] H. A. Bachor and T. C. Ralph, *A Guide to Experiments in Quantum Optics* (Wiley, New York, 2004).